Journal

Cavitation Contributes Substantially to Tensile Creep in Silicon Nitride

William E. Luecke,*,† Sheldon M. Wiederhorn,*,† Bernard J. Hockey,‡ Ralph F. Krause, Jr.,*,‡ and Gabrielle G. Long*,‡

Materials Science and Engineering Laboratory, and Ceramics Division,
National Institute of Standards and Technology,
Gaithersburg, Maryland 20899

During tensile creep of a hot isostatically pressed (HIPed) silicon nitride, the volume fraction of cavities increases linearly with strain; these cavities produce nearly all of the measured strain. In contrast, compressive creep in the same stress and temperature range produces very little cavitation. A stress exponent that increases with stress ($\dot{\varepsilon} \propto \sigma^n$, $2 < n < 7$) characterizes the tensile creep response, while the compressive creep response exhibits a stress dependence of unity. Furthermore, under the same stress and temperature, the material creeps nearly 100 times faster in tension than in compression. Transmission electron microscopy (TEM) indicates that the cavities formed during tensile creep occur in pockets of residual crystalline silicate phase located at silicon nitride multigrain junctions. Small-angle X-ray scattering (SAXS) from crept material quantifies the size distribution of cavities observed in TEM and demonstrates that cavity addition, rather than cavity growth, dominates the cavitation process. These observations are in accord with a model for creep based on the deformation of granular materials in which the microstructure must dilate for individual grains to slide past one another. During tensile creep the silicon nitride grains remain rigid; cavitation in the multigrain junctions allows the silicate to flow from cavities to surrounding silicate pockets, allowing the dilatation of the microstructure and deformation of the material. Silicon nitride grain boundary sliding accommodates this expansion and leads to extension of the specimen. In compression, where cavitation is suppressed, deformation occurs by solution–reprecipitation of silicon nitride.

I. Introduction

SILICON NITRIDE is attractive as a structural material for high-temperature applications because of its high strength, moderate toughness, and good oxidation and creep resistance. Failure by creep rupture, the accumulation of damage in the form of cavities, often determines the upper-use temperature for potential applications. Since the accumulation of damage ultimately leads to failure, it is important to understand the nature of the damage process to determine strategies to improve high-temperature lifetime. Many studies (for example, Refs. 1–9) have characterized the tensile creep behavior of various silicon nitrides at elevated temperatures. Other studies have examined the nature of creep-induced damage at high temperatures, most notably those by Lange *et al.*,[10] who measured cavity volume fractions produced by compressive creep, and those by Page *et al.*,[11–13] who studied the cavity size distributions produced by

compressive creep in SiC and alumina by small-angle neutron scattering (SANS). Because typical high-temperature, high-stress applications for silicon nitride (e.g., turbine rotors) will involve tensile stresses, and because the creep response of silicon nitride is not the same in tension and compression,[7,14] this study attempts to extend these studies to understand the evolution of damage during tensile creep. Elements of this work have appeared in two conference proceedings.[15,16] This paper extends these findings while adding a more detailed discussion not possible in the restricted conference proceedings format.

To characterize more fully the contribution that cavitation makes to the creep of Si_3N_4, this study employs several complementary techniques. The creep response of this study's Si_3N_4 was first characterized in both tension and compression. In addition, a limited number of experiments gave information on the strain relaxation behavior. Precision density measurements of the gauge lengths of crept specimens quantified the overall volume fraction of cavities that creep produced. Transmission electron microscopy revealed the location of the cavities within the microstructure as well as qualitative information on their relative sizes. Finally, small-angle X-ray scattering (SAXS) from the same specimens provided cavity size distributions that helped identify the nature of the cavity evolution.

II. Experimental Details

(1) Material

The silicon nitride of this study (Norton/TRW NT154, vintage 1991)§ is hot isostatically pressed, and contains 4 wt% Y_2O_3 as a densification aid. It is a member of the group of silicon nitrides commonly called *in situ*-reinforced composites, because their microstructures consist of large, acicular $\beta\text{-}Si_3N_4$ (here up to 10 μm long by 1 μm in diameter) grains whose interstices are filled with smaller, equiaxed grains and the residual silicate densification aid. In this silicon nitride, the second-phase glass in these interstitial regions is nearly completely crystallized to form $\alpha\text{-}Y_2Si_2O_7$[8,17] and $Y_5(SiO_4)_3N$.[8] Like most other silicon nitrides densified with the aid of a silicate glass, an amorphous grain boundary film about 1 nm thick remains on nonspecial boundaries after all heat treatments. Several other investigators have described the microstructure of this grade of silicon nitride in great detail.[1,8,17,18]

(2) Creep Testing

In the creep apparatus, a pneumatic cylinder applies the load to the specimen via SiC pull-rods. A pin and clevis arrangement transfers the load from the pull-rod to the specimen. The uniform-temperature hot zone of the air-filled furnace surrounds the entire specimen. Optical pyrometry of the furnace cavity during testing indicated that the specimen and pull-rod temperatures were the same to within 1°C. When the specimen breaks,

a microswitch at the top of the load train cuts power to the furnace to minimize postfailure annealing. The tensile creep specimens are similar to those that Carroll[19] describes, but with a second reduction in width in the gauge length, giving them a 2 mm × 2.5 mm cross section. Figure 1 shows the shape and dimensions of the specimens tested. Reference 19 describes the tensile creep testing procedure in greater detail.

A laser-extensometry system (Model 1100, Zygo Corp., Middlefield, CT) measures the strain produced by tensile creep. The strain measurement system rapidly scans a laser beam parallel to the creeping specimen through a slot cut in the furnace wall. A pair of silicon carbide flags (also shown in Fig. 1), suspended by their own weight from the specimen, interrupt the beam about 5 mm from the specimen edge. After exiting the furnace, the beam strikes a photocell sensor. From the time between the interruptions of the laser scan by the flags, the measurement unit calculates the distance between the edges of the flags. The system can reliably detect length changes of several micrometers in a typical gauge length of 8–10 mm. The flag technique introduces several potential errors into the strain measurement that conspire to limit the accuracy of the measured strain to about ±10%. A separate paper[20] details the origins of these errors as well as strategies to combat them.

Compression specimens for this study came from sections of the flanges of already-tested tension specimens. Typically, the specimens were not more than 5.5 mm tall, with a 5 mm^2 cross-sectional area. Rather than using the laser extensometry system to measure creep, we measured, using a telescope focused near the specimen, the distance between two SiC fibers attached to the platens of the compression fixture, as Ref. 21 describes in detail. The length change of the specimen measured by this technique is uncertain to about 5 μm. In a typical experiment lasting several weeks, two investigators made several length measurements each day consisting of 10–15 individual determinations of the fiber positions. Generally, different investigators made gauge-length measurements that agreed to within the uncertainty of an individual's measurement.

(3) Density Measurement

The sink-float density measurement device used to determine the cavity volume fractions is a modification of the apparatus described by ASTM standard C729.[22] Gasdaska[23] and Chen[24] have also recently used this technique to measure cavity volume fractions in a different silicon nitride. Lange[10] used a variant of this technique to make some of the first cavity volume fraction measurements in silicon nitride. In the precision density measurement apparatus, a borosilicate glass-jacketed tube contains a mixture of CH_2I_2 and $C_2H_2Br_4$, whose density is approximately that of the silicon nitride in question (here 3.225 ± 0.01 g/cm^3). By adjusting the temperature of the solution with a constant-temperature water recirculator, we can bracket the neutral buoyancy temperature. The temperature coefficient of the density solution, determined for each day's run, is calibrated by two floats of known density (R. P. Cargille Laboratories,

Cedar Grove, NJ) certified to ±0.0005 g/cm^3. Knowing the temperature coefficient of the solution, the density of the unknown can be determined by interpolation. Over the limited temperature range in question (10–50°C), the density of the solution is linear with temperature to within 0.0002 g/cm^3.[25] Typically, the uncertainty in the neutral buoyancy temperature of the specimen, determined as half the difference between the temperature at which the specimen sank upon increasing the temperature and that at which the specimen floated to the surface upon lowering the temperature, was less than ±0.075°C, yielding an uncertainty in the density of ±0.0005 g/cm^3.

Before the density determination, we removed approximately 50 μm of material from all of the exterior surfaces of the specimen, except the fracture surface. Any oxide remaining on the specimen will lower the apparent density, yielding artificially high estimates of the cavity volume fraction. To ensure that the measurement of the cavity volume fraction represents the bulk behavior of the creep specimen, we used as much of the gauge length as possible. Since the specimens usually broke near one end, these sections were typically 10 mm long. To minimize the possibility of trapped gas bubbles remaining on the surface, we polished all surfaces, again, except the fracture surface, to a finish equivalent to 6 μm diamond paste. To account for the effect of chemically induced changes during high-temperature exposure, we always determined the density of an approximately equally sized section taken from the grip-end of the same specimen. These specimens were always nominally 12 mm × 1.85 mm × 2.4 mm. The volume fraction of cavities in the tested specimen, f_v, is then

$$f_v = \frac{\rho_{grip} - \rho_{gauge}}{\rho_{grip}} \qquad (1)$$

where ρ_{grip} is the density of the grip section, and ρ_{gauge} is the density of the gauge section in question. Equation (1) assumes that all the density change in the gauge length comes from cavitation and that the cavitation is closed to the surface. It also assumes that any long-range density changes, caused for example by out-diffusion of the sintering aids in response to the oxidation, are either insignificant or canceled by the similar geometries of the gauge and grip specimens. Of course, if there are spatial variations in the starting density through the specimen, use of Eq. (1) may introduce slight error, since the grip and gauge section densities will not be identical at the start of the experiment.

(4) Transmission Electron Microscopy

Standard ceramographic techniques were used to obtain samples from gauge sections of crept samples and from grip ends of tensile samples. In all cases, crept samples, whether tensile or compressive, were cut parallel to the applied stress axis to provide cross-sectional views. As the width of the TEM sample was 2.5 mm, the edge of the creep sample was retained on the 3-mm disks used for TEM, allowing identification of the stress axis during observation.
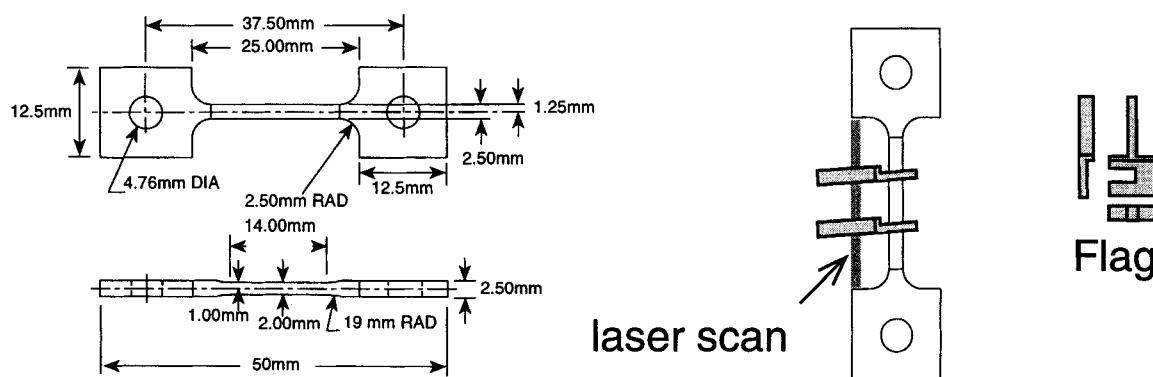

Fig. 1. The tensile creep specimen used in this study. All dimensions are in millimeters. The figure also shows the shape and method of attachment of the SiC flags that define the gauge length.

(5) SAXS Analysis

Small-angle X-ray scattering[26,27] provided information about the cavity size distributions in the crept specimens. Since all inhomogeneities (interfaces, dislocations, etc.) in the specimen scatter X-rays, we employed the same blank technique as in the precision density measurements. In every case, the specimen had been first characterized by the sink–float technique for total cavity volume fraction. After SAXS characterization, most specimens were further thinned and examined in the TEM. The SAXS specimens were thin sections sawed and ground from the center of each gauge and grip pair, with final dimensions approximately 2.5 mm × 10 mm × 0.1 mm. The scattering data collection took place at the NIST high-resolution SAXS instrument[27] at the National Synchrotron Light Source, using 0.124-nm X-rays, where the size range measured is typically 0.01–1 μm, which is somewhat broader than the range in traditional small-angle scattering (1–100 nm). The cavities and other inhomogeneities in the specimen scatter a small component of the incident beam out of the straight-through direction, and the instrument's photodiode detector[28] measures the intensity of this singly scattered beam. The raw data were placed on absolute scale[27] and slit-desmeared[27] to yield small-angle scattering cross section, $d\Sigma/d\Omega$, as a function of scattering wave vector, Q ($|Q| = (4\pi/\lambda) \sin \theta$, where 2θ is the scattering angle, and λ is the incident X-ray wavelength). The $d\Sigma/d\Omega$ vs Q data were analyzed in terms of cavity volume fraction distribution, for both gauge and grip specimens, using a maximum entropy analysis,[29–31] assuming that most of the scattering contrast is

between the silicon nitride and the cavities. The subtraction of the contribution of scatterers from the grip specimen from that of the gauge specimen yielded the contribution from the cavities alone.

III. Results

We divide the presentation of the results into three parts. The first summarizes the general creep properties of the material, focusing on specimens that crept until failure. The second presents information on the microstructure of the crept specimens, in particular the volume fraction, morphology, and distribution of cavities that form during creep. The third details results on the evolution of cavitation damage with strain.

(1) Creep Behavior

(A) Tension: Except for the suite of interrupted tests that Section III(3) describes, all of the specimens crept until failure under a single temperature and stress. Few of the specimens showed definitive steady-state creep; rather, the creep rate of most specimens continued to decrease until failure. Typically, the initial creep rate was 4 times that of the creep rate at failure, but the ratio correlates with neither temperature nor applied stress. Several specimens that crept to more than 1% strain did exhibit a roughly constant creep rate for the last half of their lives. Only one specimen of 24 tested showed any behavior that might be interpreted as tertiary creep. Figure 2 illustrates the creep curves for most of the specimens tested. In general, higher
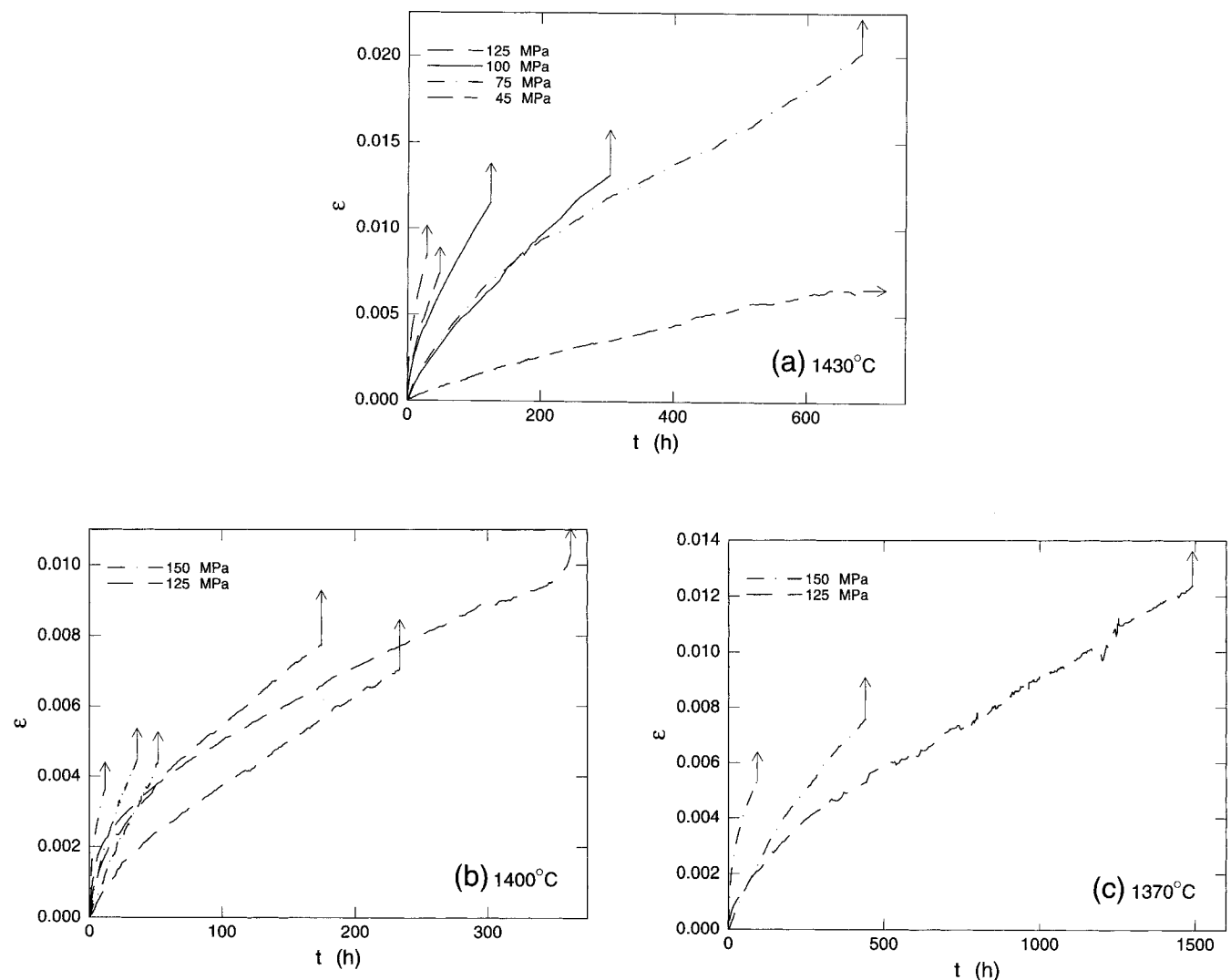
Fig. 2. Creep curves from all testing conditions: (a) 1430°, (b) 1400°, (c) 1370°C. The figures omit some of the high-stress, short-time curves for clarity. Upward arrows denote failure; horizontal arrows denote interruption before failure. Note the different time and strain axes in each plot.
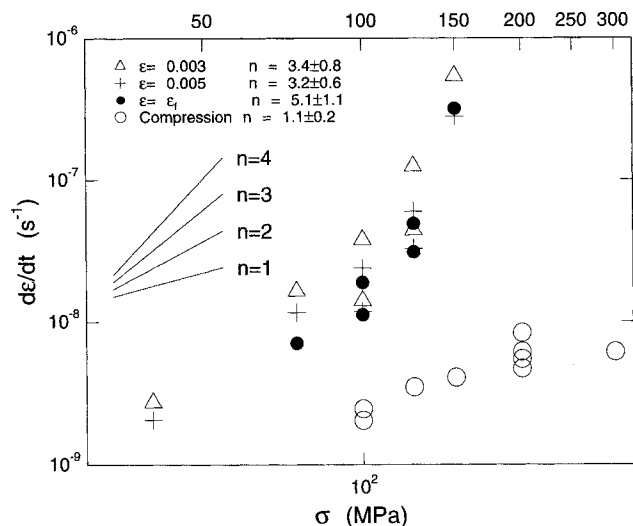
Fig. 3. Strain rate as a function of stress for tests conducted at 1430°C. The extra data points for the low strains come from tests at low stress that were discontinued before failure.
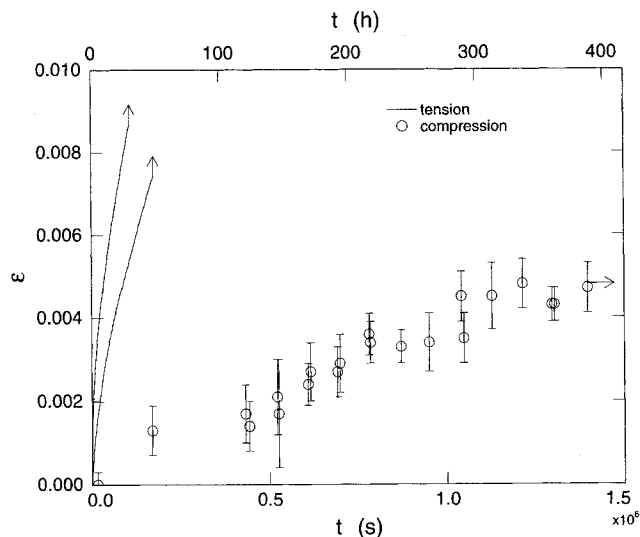

Fig. 4. Comparison of the creep curves in tension and compression for deformation at 125 MPa, 1430°C. Error bars in the compression curve represent the standard deviation of the group of 10 measurements of the specimen length. To facilitate comparison, the sign of the compressive strain has been reversed.

stresses produced shorter strains to failure. When comparing tests at the same stress, specimens tested at 1370°C showed a slightly larger strain-to-failure than those tested at 1400° and 1430°C.

The lack of steady-state creep complicates the analysis of the stress dependence of the strain rates. As will be shown later, the decay in creep rate correlates better with strain than with time, so it seems reasonable to plot the strain rate vs stress at constant values of strain, rather than the potentially arbitrary failure time. To calculate the values of the strain rate, we first took the point-by-point derivative of the strain vs time data to produce strain rate vs time data. We then combined this curve with the original curve to produce a strain rate vs strain curve. Since the point-by-point derivatives produced this way were quite noisy, to extract the strain rates we fitted to the data the parameters of a three-term model,

$$\dot{\varepsilon} = \dot{\varepsilon}_s + \dot{\varepsilon}_p[\exp(-\varepsilon/\varepsilon_0)] \tag{2}$$

where $\dot{\varepsilon}_s$ is a "secondary" creep rate, $\dot{\varepsilon}_p$ is a "primary" creep rate, and ε_0 is the strain equivalent of a time constant. Equation (2) has the form of a creep transient that decays to a constant rate over a strain of ε_0. We must emphasize that this equation represents the data in a purely phenomenological manner only, so that it is possible to extract the strain rates from the data. In general, the fits using Eq. (2) were quite good.

Figure 3 shows that as the stress increases, the slope of the strain rate–stress curve also increases. A linear fit to the low-stress half of the $\varepsilon = 0.003$ data ($40 \le \sigma \le 100$ MPa) yields a stress exponent of 2.3 ± 0.7,[1] while a fit to the high-stress half ($100 \le \sigma \le 150$ MPa) yields a stress exponent of 7.3 ± 2.0. Similar behavior obtains at the other two test temperatures, though the data from tests at 1370°C are more scattered. In all cases, though, calculation of the strain rate dependence on stress using the strain rates at failure inflates the computed value of the stress exponent. Stress relaxation studies on other HIPed silicon nitrides have yielded similar strain rate–stress curves.[33]

A similar calculation can be made for the temperature dependence of the strain rate at different strain increments, though only for two different stresses (150 and 125 MPa). Table I summarizes the apparent activation energy for creep, Q_{creep}, at several strain increments, including the failure strain, ε_f. At a given stress, the scatter in the measured creep rates produces

large uncertainties in the calculated temperature dependence. As a result, at fixed stress, the apparent activation energies, Q_{creep}, at different strain increments are not significantly different statistically, at the 95% confidence level, as determined by a t-test. However, the temperature dependence at 150 MPa is statistically significantly different from that at 125 MPa. The high-temperature dependence is in accord with those measured by other investigators on similar silicon nitrides.[3,23,34]

(B) Compression: It is difficult to assess the true shape of the compressive creep curves, due mostly to the slow creep rates and limited resolution of the telescope technique for measuring the displacement. Figure 4 compares the strain vs time curves for two tensile specimens with that of a compression specimen, all tested at 1430°C and 125 MPa. Clearly the creep rate in compression is much lower than that in tension. At a strain of 0.005, approximately the final strain of the compression experiment, the creep rates for samples in tension are almost 100 times greater than that in compression. Whether the specimen tested in compression shows a decreasing creep rate with increasing time is less clear. Linear fits to the first and last halves of the data indicate that the creep rate decreases to half its initial value over the length of the test, in comparison to the typical 4-times decrease exhibited by the specimens deformed in tension.

Figure 3 also shows data for creep in compression at 1430°C. Whereas the strain rate dependence on stress in tension is strong, and nonlinear on a log–log plot, the compression data show a stress exponent of about unity. With the exception of the single-stress experiment described in the previous paragraph, all the other compressive strain rate–stress data shown in Fig. 3 come from specimens tested under multiple stresses. The extremely slow creep rates in compression, typically 10–100 times smaller, necessitated this less-than-ideal procedure. Further complicating direct comparison between tension and compression results is the fact that compressive creep was only

Table I. Temperature Dependence of Creep in NT154

ε	Q_{creep} (kJ/mol)	
	125 MPa	150 MPa
0.001	1055 ± 377	1369 ± 561
0.003	1002 ± 255	1485 ± 309
0.005	988 ± 188	1453 ± 189
ε_f	1246 ± 117	1615 ± 170

[1]In this paper, the uncertainty following a parameter determined from a linear fit to data is the standard uncertainty as defined by Ref. 32, that is, the estimated standard deviation of the parameter.
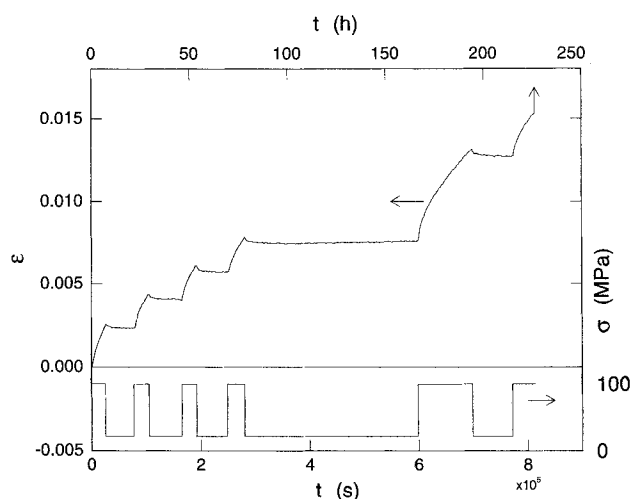
Fig. 5. Loading/unloading strain curve for a specimen deformed at 1430°C and 100 MPa.

Fig. 6. Total volume fraction of cavities in the gauge length for all specimens tested to failure.

appreciable at the highest test temperature, 1430°C. At lower temperatures the creep rate was lower than the resolution of the measurement technique, indicating that the temperature dependence of the creep rate in compression is at least as large as that in tension.

(C) Strain Relaxation: Two strain-relaxation experiments helped assess the contribution of anelastic (i.e., recoverable, time-dependent) deformation to the total strain in tension. Figure 5 shows a loading/unloading curve for a specimen deformed at 1430°C and 100 MPa, along with the corresponding stress history. In the figure, the instantaneous length changes on loading and unloading caused by elastic strains and shifts of the loading train have been removed. Table II summarizes the relevant data for both experiments. At 1430°C there is no significant dependence of recovered strain on either initial strain or total strain. The total strain recovered remained constant at about 0.0003, even with prestrains as large as 0.005. At 1400°C, the recovered strain increases slightly with prestrain, as well as increasing with total strain. Very little strain is recovered in either case.

(2) Cavitation

(A) At Failure: Figure 6 shows the volume fraction of cavities, computed from Eq. (1), as a function of failure strain. The vertical error bars in Fig. 6 represent the errors arising from the uncertainties in the densities of the calibration standards and the uncertainty in the neutral buoyancy temperature. The horizontal error bars represent an estimate of the uncertainty in the strain, here set to 10% of the total strain. The volume fraction of cavities, to a good approximation, is linear with the failure strain, with a slope of 0.93. Since the bulk of the uncertainty lies in the strain measurement rather than the cavity volume fraction (see Section II(2)), the straight-line fit to the
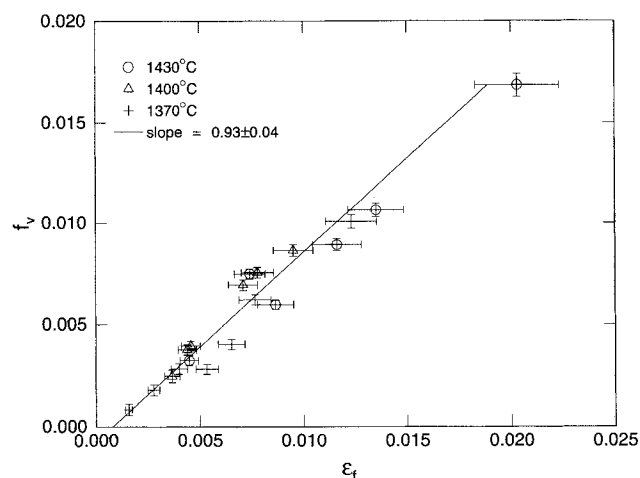
data shown in Fig. 6 is actually ε_f regressed on f_v, weighted by the estimated uncertainty in ε_f (i.e., $w_i = 1/(0.1\varepsilon_{f_i})^2$). Note that the best-fit line intercepts the negative f_v-axis, consistent with the existence of the small anelastic strain also measured. There are systematic deviations from the best-fit line, however. Most of the specimens tested at 1400°C lie above the best-fit line, while those tested at 1430° and 1370°C lie below. In addition, there is a general increase in the ratio f_v/ε_f with increasing strain for all specimens, also consistent with the existence of the small anelastic component of strain, an aspect to which we will return in the Discussion section.

To assess the homogeneity of the cavitation along the gauge length, we sectioned the gauge section of a specimen of known cavity volume fraction into six 1.5-mm-long pieces along the gauge length and redetermined the density of each piece. There was a continuous, monotonic decrease in the density of the individual sections, corresponding to an increase in cavity volume fraction, beginning with the section that originated 10 mm from the fracture surface. The difference in cavity volume fraction between the densest and least-dense sections was about 10%, indicating that the cavitation was fairly uniformly distributed along the gauge length, with only a slight increase at the end containing the fracture surface. Most of the other specimens showed a similar behavior in that they floated fracture surface up during the density determination, indicating that fracture occurred in the region of greatest cavity volume fraction.

(B) Cavity Shapes and Locations: Although the total volume fraction of cavities remained proportional to the strain, regardless of testing temperature and stress, two different types of cavities appeared, depending on temperature. In specimens tested at 1370°C, TEM of the failed specimens revealed the presence of two types of cavities. More numerous were small (100–200 nm) lens-shaped cavities that usually lay on two-grain boundaries with normals approximately parallel to the tensile axis. Less common were large (0.2–0.7 μm), irregularly shaped cavities located at multigrain junctions, typically in the pockets of equiaxed, sub-micrometer-sized grains of Si_3N_4 and crystalline silicate. The small, lens-shaped cavities tended to occur more frequently on tensile boundaries in specimens crept at high stress, which therefore exhibited small failure strains. In specimens that crept at low stress, with correspondingly larger failure strains, the distribution of the lens-shaped cavities was more random with respect to the tensile axis. In both high and low failure-strain tests, the lens-shaped cavities were distributed inhomogeneously throughout the gauge length. Typically, a cavitated grain boundary contained 10 to 20 individual cavities of similar size, while the vast majority of two-grain boundaries remained cavity free.

In contrast, specimens crept at temperatures 1400°C and higher showed very few of the lens-shaped cavities. When these

Table II. Relaxation Data from Two Experiments Conducted at 125 MPa

T	Order	ε_{pre}	ε_{relax}
1430	1	0.0025	0.0003
	2	0.0021	0.0004
	3	0.0019	0.0003
	4	0.0019	0.0002
	5	0.0054	0.0003
1400	1	0.0013	0.0002
	2	0.0014	0.0004
	3	0.0026	0.0003
	4	0.0028	0.0006
	5	0.0037	0.0006

cavities did occur, usually only a single lens-shaped cavity appeared on a boundary, in contrast to the 20 or more per boundary in specimens crept at 1370°C. The bulk of the cavities were the large, irregularly shaped, multigrain-junction type. Invariably the multigrain-junction cavities filled the entire interstitial region in which they were located. Figure 7 is a collection of transmission electron micrographs from deformed specimens that illustrates most of the features of the cavity size and shape distributions.

(C) Cavity Size Distributions at Failure: Small-angle X-ray scattering provided quantitative information on the size distribution of cavities. Figure 8 shows the volume fraction distributions from both the gauge section and grip (i.e., undeformed, but exposed for the same time and temperature) section of a single specimen. The one acquired from the gauge section of the specimen includes the contribution of all scatterers, including cavities, while the one from the undeformed grip-end of the specimen, which is known (by TEM) to be relatively cavity-free, includes only those scatterers assumed to be common to both sections. The difference of the two curves is thus the volume fraction of cavities in the gauge section. For all the specimens examined using SAXS, the total cavity volume fraction calculated by SAXS agreed with that from the precision density measurement to better than 25%. The agreement between the two techniques was better for larger cavity volume fractions. The two peaks in the cavity distribution in Fig. 8, correspond to the cavity size range observed in the TEM. Although it might appear that the peak at 0.3 μm arose from the lens-shaped, two-grain boundary cavities, TEM indicated that

there were very few small lens-shaped, two-grain-boundary cavities in this specimen. The peak must, therefore, arise from the smaller multigrain-junction cavities. For specimens which did exhibit both the lens-shaped cavities and the multigrain-junction cavities, it is not possible to assess the relative contribution of each type, since the size range of the two cavity types overlaps.

(3) Evolution

It is tempting to interpret Fig. 6 as a map of the evolution of cavity volume fraction with strain, but that figure is actually a plot of one dependent variable against another, since the different testing conditions are hidden. To ascertain the evolution of the cavitation with strain, we conducted a series of experiments at a single test condition: 1400°C, 125 MPa, interrupting the specimens before failure. In this way we were able to characterize the resulting specimens first by the density technique, then by SAXS, and finally by TEM. In an ideal experiment it would be possible to determine the cavity volume fraction at various stages during the creep process on an individual specimen. The precision density technique, as well as SAXS and TEM, requires destruction of the creep specimen, making determinations on multiple specimens crept to various strains a necessity.

(A) Volume Fraction Evolution: Figure 9 shows the evolution of total cavity volume fraction with strain for four specimens tested at 1400°C and 125 MPa and interrupted before failure, as well as five specimens tested to failure under those conditions. Not only does the cavity volume fraction evolve
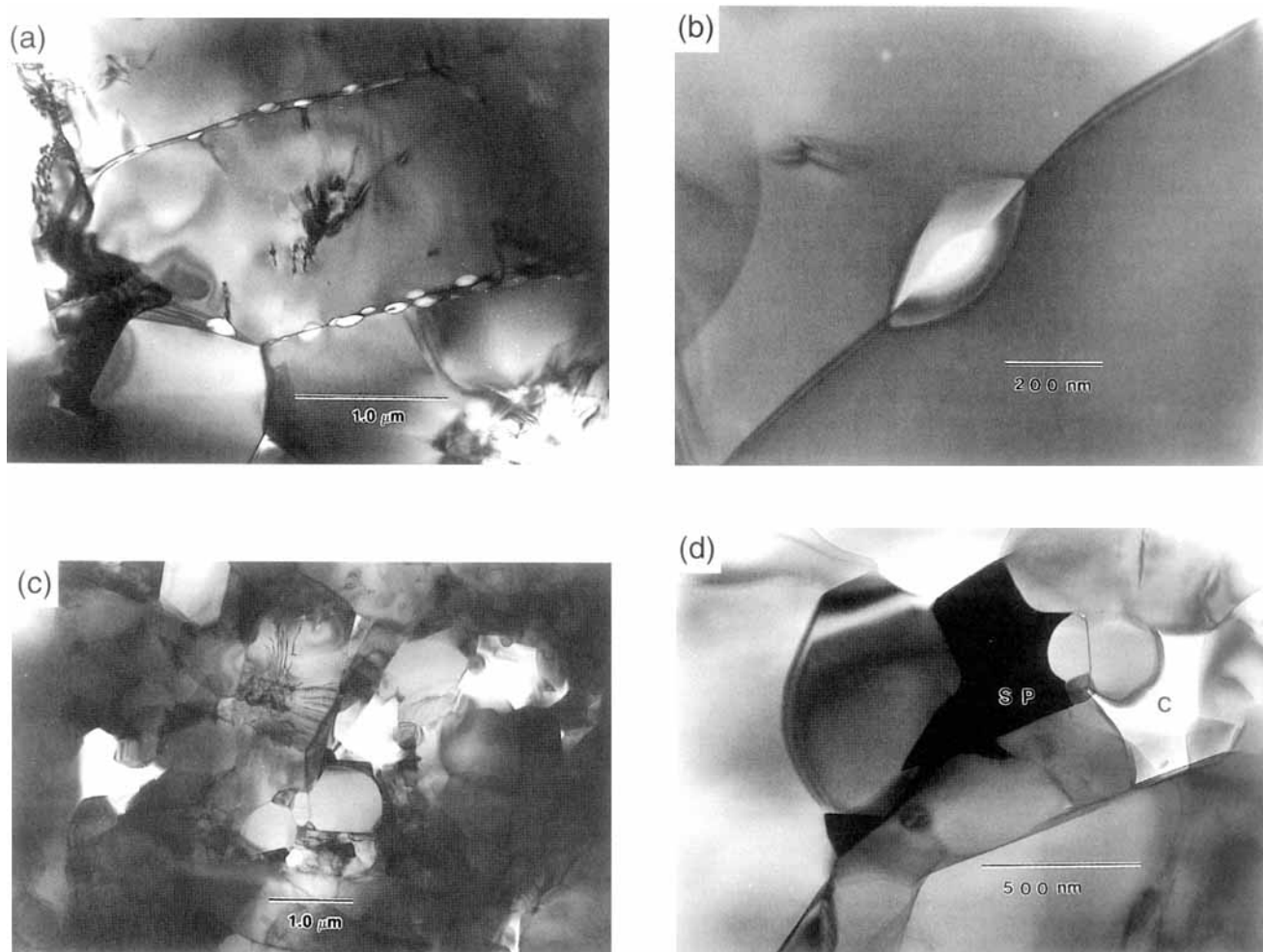
Fig. 7. Transmission electron micrographs showing both small, lens-shaped cavities as well as the larger, more irregularly shaped cavities. (a) and (b) show the lens-shaped cavities that formed in a specimen crept at 1370°C under 125 MPa for 1521 h, while (c) and (d) show the irregularly shaped, interstitial cavities that formed in the silicate phase in a specimen deformed at 1430°C under 125 MPa for 30 h. In both micrographs the tensile axis is vertical. In (d) "C" is a cavity and "SP" is the silicate phase.
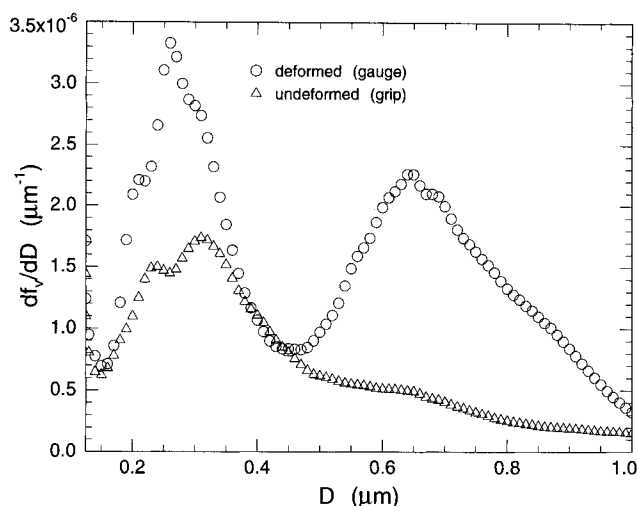
Fig. 8. Derived cavity volume fraction size distributions for a specimen tested to failure at 1430°C and 100 MPa. The difference between the curves is the cavity volume fraction distribution for the specimen.

linearly with increasing strain, but the volume fractions of cavities in the unfailed specimens lie close to the line defined by the complete data set of all failed specimens for all temperatures and stresses (Fig. 6).

(B) Cavity Size Distribution Evolution: Figure 10 shows the evolution of the volume fraction distribution of cavities, characterized by SAXS, as a function of strain for three of the four interrupted-before-failure specimens from Fig. 9, as well as from a specimen allowed to creep until failure. We omit the data from the specimen tested to the smallest strain for clarity.

(C) Cavity Shape and Distribution Evolution: Transmission electron microscopy of several of the specimens interrupted before failure and characterized by the density technique (Fig. 9) and SAXS (Fig. 10) confirmed qualitatively the observations of both. With increasing strain, the number of large, multigrain-junction cavities increased. One specimen (ε = 0.0064 in Fig. 10) did show some of the lens-shaped, two-grain-boundary cavities, but the remaining specimens in this set showed very few.

IV. Discussion

There are several points on the interpretation of the results that warrant discussion before launching into a more general discussion of creep of this material.
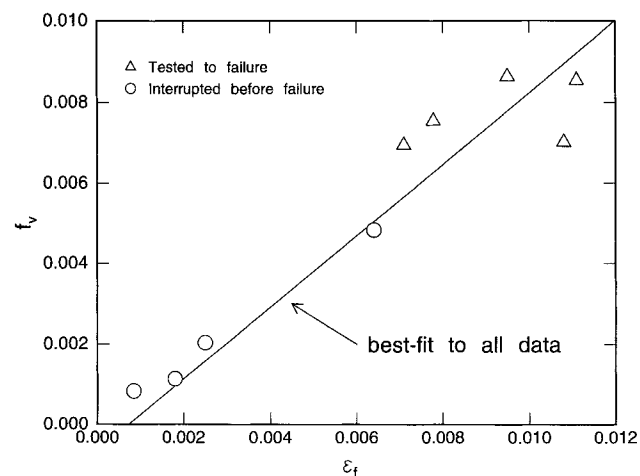

Fig. 9. Volume fraction of cavities as a function of strain for specimens crept at 1400°C and 125 MPa, along with the best-fit line from Fig. 6.
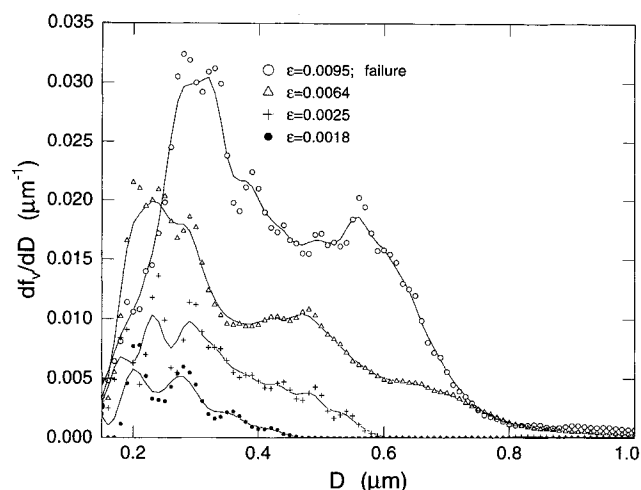

Fig. 10. Cavity size distribution evolution as a function of strain for specimens crept at 1400°C and 125 MPa.

(1) Shapes of Creep Curves

It is indisputable that the creep curves show an extended primary regime, in common with many other silicon nitrides.[1,3,7,9,23,35-37] Lange et al.[38] attributed the extended primary to a "cleaning effect" in the grain boundary phase, occurring when its cations diffuse from the interior of the specimen to the surface oxide. During oxidation, the surface oxide that forms is relatively depleted in the cations of the grain boundary phase, so there exists a chemical potential gradient for the cations between the interior and the surface. In response, the more mobile cations (presumably those which also lower the viscosity of the second phase) diffuse out to the surface. Haig et al.[39] and Gasdaska[23] attributed the primary regime to anelastic effects caused by elastic loading of the silicon nitride grains during grain boundary sliding.

For NT154 neither the "cleaning-effect" nor the anelastic response of the material provides an explanation for the observed primary creep. At each test temperature the primary regime appeared, regardless of the length of the test. If the high-temperature exposure had been responsible for the primary creep, specimens tested at high stress, with correspondingly low failure times, would not have showed the primary creep. For example, after a 24-h, no-stress preanneal, a specimen tested at 150 MPa and 1430°C that failed in 2.2 h with ε_f = 0.0045 showed a primary creep regime as strong as a specimen crept at 1430°C, 100 MPa that failed after 126 h at ε_f = 0.0116. Furthermore, replicate studies done at 1400°C and 125 MPa[40] showed that a no-stress preanneal for 700 h of the creep specimens prior to loading did not remove the primary creep regime.

The data from the strain relaxation tests (Fig. 5 and Table II) and the cavity volume fraction evolution data (Fig. 9) rule out anelasticity as the sole source of the primary creep. We can choose to represent the creep data by the standard viscoelastic model[41]—a Kelvin element (spring and dashpot in parallel) in series with a dashpot. Here the Kelvin element represents the anelastic strain element, while the line dashpot represents the creep strain. In such a representation the creep strain as a function of time is

$$\varepsilon(t) = \dot{\varepsilon}_s t + \varepsilon_0[1 - \exp(-t/\tau)] \tag{3}$$

where $\dot{\varepsilon}_s$ is the secondary creep rate, ε_0 is the strain at which anelasticity ceases to contribute to the strain, and τ is the time constant for relaxation. The strain-relaxation data collected at 1430°C (Table II) indicate that the recovered strain is fairly independent of the prestrain and averages $(3.1 \pm 0.8) \times 10^{-4}$ with an average time constant $\tau = 8100 \pm 2500$ s. For the two experiments conducted at 1430°C and 100 MPa, the ε_0 parameter averages 2.5×10^{-3}, nearly 10 times the strain recovered on unloading. For the 1400°C experiments the ε_0 parameter

averages to 2.2×10^{-3}, nearly 5 times the recoverable strain. The cavity volume fraction evolution experiments (Fig. 9) make the strongest reinforcement of this point, since they show that the cavity volume fraction makes an equal and substantial contribution to the overall strain regardless of the amount of creep strain, indicating that the primary creep has its origin in the cavitation process, rather than in an anelastic process.

(2) Contribution of Cavities to Creep Strain

The precision density measurements of cavity volume fraction in specimens interrupted before failure (Fig. 9) show that the cavity volume fraction increases linearly with strain, but they do not distinguish between cavity growth and cavity addition, since both mechanisms produce an increase in cavity volume. Fortunately, the SAXS analysis of the same specimens provides the missing information: cavity addition dominates the strain production.

During creep, two peaks develop in the volume fraction distributions in Fig. 10. One peak is centered at about 0.25 μm, while the other appears first as a shoulder on the first peak. Although it contributes very little volume fraction at small strains, this shoulder eventually grows to contribute nearly half the volume fraction of cavities by failure. For small strains, i.e., during the primary creep regime, the area under the peak at 0.25 μm increases, but the peak does not shift, implying that creep is adding new cavities of this size. The TEM investigation confirms that this peak results from scattering by the smaller multigrain-junction cavities, as the lens-shaped two-grain-boundary cavities do not form in great numbers at 1400°C. During the primary creep the shoulder also grows, both by shifting position to larger diameters as well as by increasing in area. Figure 11, a plot of cavity number density vs strain, shows that the addition of new cavities, rather than growth of existing cavities, dominates the cavitation process. During primary creep (ε (or f_v) < 0.005), the number of cavities in both the peak at 0.25 μm as well as that in the shoulder increases linearly with volume fraction (i.e., with strain). As the creep rate slows down into the secondary regime, the number of cavities only increases slightly, implying that growth of existing cavities is making a more significant contribution to the total volume fraction. In any case, however, the addition of new cavities contributes more to the total volume fraction of cavities than does growth of existing cavities.

Since it is impossible to follow the development of an individual cavity, whether by TEM or SAXS, it is not possible to unambiguously link growth of the shoulder in the SAXS data

Fig. 11. Number of cavities as a function of volume fraction for specimens tested at 1400°C, 125 MPa. The cavity volume fractions in the figure come from the precision density measurements. The plot shows total cavities as a function of strain (N_{total}) as well as those with diameters less than 4000 Å ($N_{D<4000Å}$).

(Fig. 10) to the growth of existing small interstitial cavities. However, it seems reasonable to assume that these large cavities are developing as a result of the growth of smaller cavities, rather than by springing fully grown into existence. It may be possible, however, that the larger cavities form as the result of the linkage of two adjacent smaller cavities, but again, it is not possible to unambiguously assert this.

(3) Creep by Dilatation

Before expounding on a model of creep to explain these observations, these are the salient experimental observations:
• Cavitation accounts for a substantial fraction of the tensile creep strain.
• The cavity volume fraction increases linearly with the total tensile strain, beginning immediately upon application of the load, even when the creep rate continuously decreases with both time and strain.
• For the bulk of the creep life, addition of new cavities, rather than growth of existing cavities, produces the bulk of the increase in cavity volume fraction.
• A large stress exponent, which increases with increasing stress, characterizes the tensile creep behavior, whereas a stress exponent of unity characterizes the compressive creep.
• The majority of the cavitation occurs within pockets of crystalline silicate phase, which are themselves located in "interstitial" pockets formed by the clusters of large silicon nitride grains.

The large stress dependence of the tensile creep rules out the possibility that simple diffusional creep models might explain the deformation. Dislocation creep models are not candidates, since the material shows insufficient evidence of dislocation activity as a result of creep. The large volume of cavities relative to the creep strain indicates that the creep is intimately tied to the cavitation process, rather than being a second-order effect, as usually seen in the creep cavitation of metals (i.e., constrained cavitation).[42]

(A)   Creep   in   Compression: The   compression   creep behavior is conceptually simpler to explain and offers a baseline to measure the tension creep results. The density experiments confirm that there is negligible cavitation during compressive creep. The unity stress exponent is powerful evidence that creep occurs by a diffusional mechanism. It seems most likely that the creep is by solution–reprecipitation of the silicon nitride from grain boundaries in compression to boundaries under tension, but in the absence of definitive grain-size experiments, it is impossible to say for certain. The existence of the lens-shaped cavities that appear at the lower temperatures during tensile creep confirms that silicon nitride can move by diffusion through the siliceous phase along the two-grain junctions. Of course, the diffusion distance for the growth of the cavities by a Hull–Rimmer process[43] (such as must operate in the growth of the lens-shaped cavities) is much shorter (on the order of several hundred nanometers) than the diffusion distance for solution–reprecipitation creep (on the order of the grain diameter—several micrometers). The extreme temperature dependence of the creep rate in both tension and compression creep is consistent with arguments made by Raj and Morgan[44] concerning the activation energy for creep by solution–reprecipitation, in which both the heat of solution of silicon nitride as well as its intrinsic diffusivity contribute to the apparent activation energy for creep.

Under special circumstances it might be possible for creep to occur simply by redistribution of second phase either diffusionally or viscously. Dryden et al.[45] with later extensions by Chadwick and Wilkinson,[46,47] Cooper,[48,49] and Lange[50] have proposed models for such creep. Wilkinson has recently termed this creep mechanism exhaustion creep, while Cooper et al. term their model dilatational creep. The applicability of the former two models to the creep of the silicon nitride in this study is questionable, however. We postpone discussion of Lange's model until Section IV(3)(B).

Dryden et al. consider the microstructure of the material to be composed of rigid grains separated by viscous fluid. In
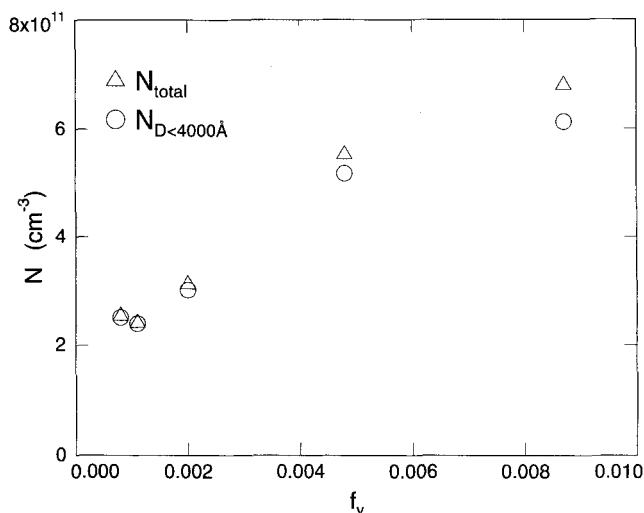
compression, the applied load squeezes out the fluid from the compressively loaded grain boundaries to the grain boundaries under tension. There is an inherent asymmetry in the creep behavior because, for example, in a microstructure composed of cubic grains, 2/3 of the grain boundaries can receive material during compression creep, but only 1/3 can during tensile creep. When the microstructure takes the form of an array of regular hexagons (in two dimensions), the creep rate in tension will be twice that in compression for long creep times.

The simplest application of the model of Dryden *et al.* to the deformation of silicon nitride is to consider that the applied load squeezes out the siliceous material lying on two-grain boundaries under compression. Even if the creep stress could squeeze out all this siliceous material, the maximum strain achievable before complete contact of individual silicon nitride grains is on the order of the ratio of grain boundary film thickness to grain diameter, or $\varepsilon = 0.001$ for 1 μm grains with 1 nm grain boundary film thicknesses. At the point of grain contact, the creep should cease, or at least slow dramatically. In the silicon nitride of this study, however, strains much larger than 0.001 commonly occur in both tension and compression with no extreme reduction in creep rate. A second aspect of the Dryden model is a continuous, substantial decrease in the creep rate with strain. As the separation between approaching boundaries decreases, it becomes more and more difficult to expel the fluid from between the grains. Four-point bending experiments conducted by Chadwick *et al.* on sintered silicon nitride, in support of the extension of the model to nonlinear viscous fluids, showed a 10-fold decrease in the compressive creep rate over the first 1% strain. No such large decrease in creep rate occurred during compressive creep of the silicon nitride in this study.

If, at high temperature, the siliceous film were thicker than that measured at room temperature, it would be possible to achieve much larger strains by the exhaustion creep mechanism. There is some evidence that the two-grain boundary film thickness may increase with temperature. Clarke's original study,[51] in which he rapidly quenched thin specimens of MgO-doped (Norton NC-132) Si_3N_4 from 1450°C, showed that after the quench from this high temperature the grain boundary film could be as thick as 10 nm. Cinibulk *et al.*[52] conducted a follow-up study, also using NC-132 as well as a noncommercial Yb-Al-doped Si_3N_4. They found that the widening of the grain boundary film appeared to be a transient phenomenon, in that the grain boundary films in specimens quenched from very high temperatures (1550°C) showed no significant thickness increase when compared to the slow-cooled specimens. They postulated that the film thickness increase occurred because of large-scale melting when the specimen temperature exceeded the eutectic temperature during heat-up. Since the specimens did not remain at high temperature for more than a few seconds, the molten glass could not redistribute before the quench, and thus remained trapped on the two-grain boundaries. The results of Cinibulk *et al.* indicate that the siliceous film thickness at room temperature is probably not too different from that at the creep temperature, ruling out exhaustion creep as the dominant mechanism in compression.

Cooper *et al.*[48,49] have considered a creep mechanism involving the transport of the second phase as well, but one in which the second phase redistributes in the triple junctions, rather than the two-grain boundaries, as a response to the applied load. Their work is concerned primarily with explaining the extended transient creep in glass-ceramics and seismic attenuation in their geologic analogues. The essence of their model is that the material contained in the grain triple-junctions (a glass or fluid) in a specimen under load feels an effective pressure, p_e, that is the difference between the average hydrostatic pressure on the specimen (($\sigma_1 + \sigma_2 + \sigma_3$)/3, where the σ_i are the principal stresses) and the pore pressure of the fluid. When the glass (or fluid) is free to communicate with the surface of the specimen inviscidly, the pore pressure is just the atmospheric pressure. The well-known relation

$$p_e = \gamma_{sl}/r \qquad (4)$$

where γ_{sl} is the solid–liquid interfacial energy, relates the effective pressure in the triple junction, p_e, to its radius of curvature, r.[53] An increase in effective pressure, produced, perhaps by compressive loading, drives the equilibrium radius of curvature down, resulting in a driving force to reduce the size of the triple junction. In partially molten systems, this pressure squeezes the melt out to the surface or to regions of lower effective pressure. Cooper *et al.* conduct their experiments in four-point bending, which requires that the melt migrate from the compression side of the specimen to the tensile side, and have recently demonstrated the redistribution of nearly 1/4 of the total volume of melt from the compression to the tension side of a specimen undergoing four-point bending creep.[49]

To make the size of the triple junction smaller, the grain centers of the surrounding grains must approach one another, a process that requires that crystalline material leave the surrounding two-grain boundaries and redeposit in the triple junction. In the partially molten systems studied by Cooper *et al.*, the melt removal step is fast, because the viscosity of the melt is low. In this case dissolution–transport–reprecipitation kinetics of the crystalline phase limit the rate of reequilibration of the microstructure to a change in stress. This type of deformation is completely recoverable; upon removal of the load the molten phase flows back to its equilibrium distribution. Because the transport of the crystalline phase along two-grain boundaries limits the rate at which this dilatational creep occurs, its contribution to the overall creep rate is similar to that produced by the steady-state, ordinary solution–reprecipitation creep. The dilatational mechanism manifests itself in the appearance of a substantial (several percent strain) creep transient during flexural creep as the molten phase redistributes.

Most important to our consideration of applicability of the Cooper model is that the deformation involved is fully recoverable, and that the dissolution–reprecipitation kinetics of the crystalline phase limit the creep rate. Although we did not attempt to measure the recoverability of the strain in compression, the Cooper model seems an unlikely candidate, in that the high effective viscosity of the crystalline silicate phase would preclude its ability to leave the triple junctions rapidly, a necessary condition for the operation of this mechanism. In addition, the tension strain-recovery experiments showed nearly negligible recoverable strain, indicating that the mechanism certainly did not operate in tension.

Since the mechanisms of Cooper and Dryden, both of which require redistribution of the second phase, do not appear to be likely candidates for compressive creep mechanisms, the most likely mechanism is that of solution–reprecipitation creep. Confirming evidence for this assertion comes from the observation of the unity stress exponent ($\dot{\varepsilon} \propto \sigma^1$) for compressive creep. The observation that lens-shaped cavities can form on grain boundaries during tensile creep indicates that the silicon nitride can diffuse along grain boundaries at the creep temperature.

(B) Creep in Tension: Clearly, the addition of cavities is central to the production of tensile strain. A question exists, however, as to whether the growth rate of the cavities limits the creep rate, or whether some intrinsic process, such as grain boundary sliding is the limiting step. In this second case the cavity simply accommodates the strain produced, rather than limiting the strain rate. In this section we will argue that the nucleation and growth kinetics of the cavities control the creep rate, rather than simply manifesting the strain created by some other process.

The discussion of Section IV(3)(A) shows that the creep rate in compression represents the maximum rate at which silicon nitride can be redistributed by solution–reprecipitation creep (i.e., a mechanism in which shape-change of the individual grains produces the bulk of the strain). Since the creep rate in tension is so large, compared to that in compression, some other mechanism must operate that allows strain without significant grain-shape change.

In 1975, in an undercited paper, Lange[50] developed a model which predicted that a polycrystal composed of rigid grains separated on all sides by viscous fluid would show an asymmetry in the creep rate between tension and compression. Like the model that Dryden *et al.* developed,[45] it extended an original model by Drucker.[54] Unlike Dryden *et al.*, Lange first established, using models first developed for adhesion theory, that in all cases, boundary separation (or approach) rather than boundary sliding would control the creep rate of such a polycrystal. Following on that conclusion, he argued that because the rate of separation of parallel plates under constant load separated by a viscous fluid depends on the fifth power of the separation distance, boundary separation will always be faster than boundary approach, leading to a large asymmetry between the tension and compression creep response. In addition, he argued that separating boundaries generally must contain a growing vapor bubble (i.e., a cavity) in order to separate, except during a short transient period during which the thick boundaries reject material to thin boundaries until all boundaries reach constant width. After this short transient, the growth of the cavities will proceed without the movement of the viscous phase to other boundaries. Instead, the viscous material remains on the cavitating boundary, in effect jacking the two grains apart.

As with the Dryden model, this sort of model is not directly applicable to the silicon nitride of this study, as the cavities do not form on two grain boundaries in tension, but in multigrain junctions. In addition, it is not possible for only some grain boundaries to cavitate if no fluid can redistribute between boundaries. Lange used a simplified microstructure that permitted sliding of stacks of grains to accommodate the growing cavity. As will be discussed below, however, tightly packed assemblages of rigid particles possess the property of dilatancy. In order for grains to slide past one another, the interstitial volume between the particles must increase, or dilate. This dilatation requires the redistribution of the fluid phase from boundary to boundary.

The requirement that an assemblage of rigid grains must dilate to deform is a well-established concept in the soil-mechanics community. Osborne Reynolds (of the Reynolds number) not only did the pioneering work,[55] but coined the term "dilatancy" to describe the property of volume expansion on shear of granular media. Reynolds himself presented the simplest natural example of the dilatancy of granular media—the fact that wet sand at the water's edge dries out when stepped upon. The water is sucked from the surface into the dilating pore space of the sand underneath the foot. A number of years later, Wroth[56] demonstrated that close-packed assemblages of ball bearings increased in volume when sheared, while loosely packed assemblages densified. Allison *et al.*[57] applied these concepts to explain the high-temperature strength of refractories. Tsai and Raj[58] recognized that glass ceramics could be dilatant in response to a shear stress, and that grain boundary sliding could produce hydrostatic tensile stresses in triple-junctions leading to cavitation. Typical silicon nitrides, including that considered here, are much more densely packed than assemblages of sand grains or ball bearings, and thus, if the silicon nitride grains remain rigid during deformation, must also be dilatant. The pore space, which is filled with crystalline silicate phase, must expand in volume if the grains of silicon nitride slide past one another rigidly.

For the creep deformation of silicon nitride, consider the case where the specimen is loaded in tension. In tension, the stress state is reversed from that in compression, in that the pockets of crystalline silicate phase find themselves initially in a state of hydrostatic tension, rather than compression. There is still the driving force for creep by a solution–reprecipitation mechanism, but the rate at which this might occur (as seen from the compression experiments) is very low. The Cooper mechanism also might operate here, but in the absence of cavitation, the diffusion distance to supply the silicate necessary to increase the size of the multigrain junctions is on the order of the sample size. In any case, because the rate at which the Cooper

mechanism contributes to the strain is tied to the motion of silicon nitride, the maximum strain rate increase is only several times that of the ordinary solution–reprecipitation mechanism, and thus cannot be the source of the hundredfold increase in creep rate seen in tension.

Consider the case, however, when some of the multigrain junctions cavitate, setting aside for the moment the actual source of the stress concentration necessary for cavity nucleation. At the surface of the growing cavity the normal stress is zero; there is, therefore, a large driving force to redistribute the silicate into the other multigrain junctions, all of which find themselves under hydrostatic tension, and thus desire to be filled with more silicate. With a ready source of silicate, the multigrain junctions can now expand, leading to creep. For small strains, the grain centers may now move apart as the silicon nitride grains slide rigidly; grain boundary sliding accommodates the dilatation. Figure 12 is a two-dimensional schematic diagram that illustrates the redistribution process. In tension, the sliding-induced hydrostatic stresses in the multigrain junctions add to the initial hydrostatic tension, since dilatancy requires the silicate pockets to increase in volume. In compression, the sliding-induced dilatancy stresses oppose the initial hydrostatic compression. There is literature evidence[10] that cavities can form in compression, but the stresses (300–500 MPa) at which they make a substantial contribution to the creep strain are much greater than those used in this study. At very high compressive stress, the hydrostatic tensile stresses generated by sliding could overcome the initial hydrostatic compression of the silicate pockets. Cavities can then form and redistribute their contents to surrounding silicate pockets, leading to creep.

A simple experiment demonstrated clearly that the grain centers must move apart if the silicon nitride grains remain rigid during redistribution of the silicate. From the gauge-length of an already-tested and characterized tensile specimen, we fabricated a compressive creep specimen, similar in size to those that Section II(2) describes. The tensile specimen from which the compression specimen came had crept to a strain of 0.0108 at 1400°C under 125 MPa during which it accumulated a cavity volume fraction of 0.0071, as characterized by the precision density measurement technique. We then loaded the specimen in *compression* under the same temperature and stress (1400°C and 125 MPa). Under these conditions the precavitated specimen did not creep, as expected from the stress and temperature dependence of the compressive creep behavior of uncavitated specimens. Compressive creep of virgin specimens only occurred at 1430°C or higher; we were unsuccessful in observing compressive creep at temperatures lower than this. In addition, to within the precision of the density technique, the cavity volume fraction remained unchanged after 400 h under load, implying that the compressive load removed virtually none of
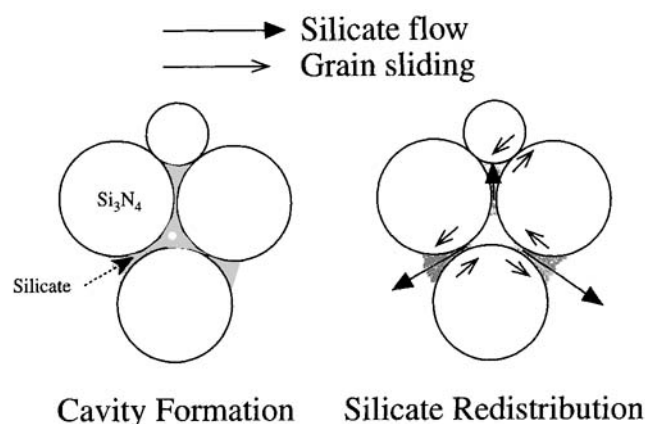
Fig. 12. Two-dimensional schematic diagram of the redistribution of silicate during cavitation. To emphasize that the silicate pockets are interconnected, the silicon nitride grains appear as circles.

the cavities. It might be expected that reversing the sign of the stress would move the silicate back into the cavities, but such motion of the silicate requires that the silicon nitride grains slide rigidly. That process, in turn, requires dilatation of the interstitial (i.e., silicate-filled) pockets. Such a dilatation would tend to generate tensile stresses in the silicate pockets, as it does during tensile creep. These tensile stresses would tend to retain the silicate in the pockets rather than allowing it to fill in the existing cavities. Redistribution of the silicate from filled pockets into existing cavities requires compressive stresses in the filled pockets, since the pockets must become smaller and the cavities are essentially at zero stress. Since rigid sliding of the silicon nitride grains during compressive creep would generate tensile stresses in the pockets, it is not possible to remove existing cavities by a compressive load of the same magnitude as that which generated the cavities. In an ideal case it might be possible to "run the whole process in reverse" and fill in each cavity in exactly the reverse order in which it formed. Given the large number of cavities formed in the gauge length, it seems impossible that this would happen, though.

The grain boundary sliding that accommodates the growing cavity tends to load new silicate pockets, leading to the continuous cavity nucleation observed in this material. Upon initial application of load, only a few silicate pockets may cavitate. The sliding accommodation of the cavity growth changes the local stress state on other pockets, perhaps even loading previously unloaded pockets. There is microstructural evidence that grain-to-grain elastic contact may resist sliding. Transmission electron micrographs from specimens quenched from high temperature under load show numerous "strain whorls" along silicon nitride two-grain boundaries. These strain whorls indicate that large elastic stresses exist between the grains, which would also tend to resist the load shedding to the uncavitated silicate pockets. Without sliding to load new multigrain junctions, cavitation is not possible, so the strain rate must decrease. Besides resisting the cavitation process, the elastic intergrain stresses could also serve as the source of the small, but measurable, anelastic relaxation. Upon removal of the load, these elastic stresses would drive the grains back whence they came. The source of the anelastic recovery may also be, as Gasdaska has suggested,[23] the unloading of strained, but uncavitated, multigrain junctions.

This resistance of the silicate pockets to cavitation can also explain the steep and ever-increasing dependence of strain rate on stress. Increasing the stress at a given temperature effectively loads more silicate pockets to stresses greater than the stress needed to cause cavitation. Since the distance over which the silicate must redistribute is decreased because of the decreased cavity spacing, creep occurs more rapidly. The decreased cavity spacing does not immediately lead to tertiary creep, though, as the loss of gauge section due to cavities is quite small for the small strains-to-failure. The stress dependence of the creep rate is not directly calculable, since it depends essentially on the distribution of grain pockets favorably oriented for cavitation. The grain boundary sliding accommodation of cavity growth may simply load new multigrain junctions as fast as they are cavitated, leading to a steady-state creep, or the number of possible cavitation sites may decrease with strain, leading to the observed long primary creep regime.

V. Summary

This study found the following important experimental observations about the creep of a HIPed silicon nitride:

• The volume fraction of cavities increased linearly with strain and accounted for a substantial fraction of the strain in tension.

• Irregularly shaped interstitial cavities made up the bulk of the total volume fraction of cavities, though at low temperatures lens-shaped, interfacial cavities were also present.

• Neither anelastic effects nor oxidation-induced chemistry changes contributed significantly to the existence of the extended primary creep regime.

• Creep added new cavities throughout the life, but growth of existing cavities began to contribute significantly to the total volume of cavities at large strains.

• While the material crept readily with a strong stress dependence in tension, it showed a hundred- to thousandfold increase in creep resistance in tension, as well as a linear dependence of creep rate on stress.

From these experimental observations we have articulated a simple creep model in which during tensile creep the grains of silicon nitride remain essentially undeformed. This rigidity requires that the silicate-filled interstitial volume of the microstructure increase in volume during deformation, leading to cavitation of the weaker silicate phase at multi-grain junctions. Cavities act as sources of silicate to feed surrounding pockets, allowing them to expand in volume. Sliding of silicon nitride grains accommodates this expansion, and, in turn, loads new silicate pockets, leading to continuous nucleation of cavities with strain. The creep rate, however, decreases with time as intergrain contact or exhaustion of suitable pockets removes the ready sources of silicate for further strain production. In compression, the inability to form cavities rules out the possibility of this mechanism, and diffusional creep produces the measured strain.

References

[1]D. C. Cranmer, B. J. Hockey, S. M. Wiederhorn, and R. Yeckley, "Creep and Creep Rupture of HIP'ed Si_3N_4," *Ceram. Eng. Sci. Proc.*, **12**, [9–10] 1862–72 (1991).

[2]J.-L. Ding. K. C. Wu, K. L. More, and C. R. Brinkman, "Creep and Creep Rupture of an Advanced Silicon Nitride Ceramic," *J. Am. Ceram. Soc.*, **77**, 867–74 (1994).

[3]M. K. Ferber and M. J. Jenkins, "Evaluation of the Strength and Creep-Fatigue Behavior of Hot Isostatically Pressed Silicon Nitride," *J. Am. Ceram. Soc.*, **75**, 2453–62 (1992).

[4]R. K. Govila, "Uniaxial Tensile and Flexural Stress Rupture Strength of Hot-Pressed Si_3N_4," *J. Am. Ceram. Soc.*, **65**, 15–21 (1982).

[5]M. G. Jenkins, M. K. Ferber, and C.-K. J. Lin, "Apparent Enhanced Fatigue Resistance under Cycling Tensile Loading for a HIPed Silicon Nitride," *J. Am. Ceram. Soc.*, **76**, 788–92 (1993).

[6]M. Kawai, H. Fujita, Y. Kanki, H. Abe, and J. Nakayama, "Tensile Testing of Sintered Silicon Carbide and Silicon Nitride"; pp. 269–78 in *Ceramic Components for Engines: Proceedings of the First International Symposium, 1983, Japan.* Edited by S. Sōmiya, E. Kanai, and K. Ando. Elsevier Science Publishing Co., London, U.K., 1986.

[7]R. Kossowsky, D. G. Miller, and E. S. Diaz, "Tensile and Creep Strengths of Hot-Pressed Si_3N_4," *J. Mater. Sci.*, **10**, 983–97 (1975).

[8]M. N. Menon, H. T. Fang, D. C. Wu, M. G. Jenkins, M. K. Ferber, K. L. More, C. R. Hubbard, and T. A. Nolan, "Creep and Stress Rupture Behavior of an Advanced Silicon Nitride: Part I, Experimental Observations," *J. Am. Ceram. Soc.*, **77**, 1217–27 (1994).

[9]T. Ohji, Y. Yamauchi, and S. Kanzaki, "Tensile Creep and Creep Rupture Behavior of HIPed Silicon Nitride"; pp. 569–74 in *Silicon Nitride 93*, Proceedings of the International Conference on Silicon Nitride-Based Ceramics (Stuttgart, Germany, October 4–6, 1993). Edited by M. J. Hoffmann, P. F. Becher, and G. Petzow. Trans Tech Publications, Aedermannsdorf, Switzerland, 1994.

[10]F. F. Lange, B. I. Davis, and D. R. Clarke, "Compressive Creep of Si_3N_4/MgO Alloys, Part 1, Effect of Composition," *J. Mater. Sci.*, **15**, 601–10 (1980).

[11]R. A. Page, J. Lankford, and S. Spooner, "Small-Angle Neutron Scattering Study of Creep Cavity Nucleation and Growth in Sintered Alumina," *J. Mater. Sci.*, **19**, 3360–74 (1984).

[12]R. A. Page, J. Lankford, and S. Spooner, "Nucleation and Early-stage Growth of Creep Cavities in Hot-Pressed Silicon Carbide," *Acta Metall.*, **32**, 1275–86 (1984).

[13]R. A. Page, J. Lankford, K. S. Chan, K. Hardman-Rhyne, and S. Spooner, "Creep Cavitation in Liquid-Phase-Sintered Alumina," *J. Am. Ceram. Soc.*, **70**, 137–45 (1987).

[14]B. J. Hockey, S. M. Wiederhorn, W. Liu, J. G. Baldoni, and S.-T. Buljan, "Tensile Creep of Whisker-reinforced Silicon Nitride," *J. Mater. Sci.*, **26**, 3931–39 (1991).

[15]W. Luecke, S. M. Wiederhorn, B. J. Hockey, and G. G. Long, "Cavity Evolution During Tensile Creep of Si_3N_4"; pp. 467–72 in *Silicon Nitride Ceramics—Scientific and Technological Advances.* Edited by I-W. Chen, P. F. Becher, M. Mitomo, G. Petzow, and T. S. Yen. Materials Research Society, Pittsburgh, PA, 1993.

[16]W. Luecke and S. M. Wiederhorn, "Tension/Compression Creep Asymmetry in Si_3N_4"; pp. 586–92 in *Silicon Nitride 93*, Proceedings of the International Conference on Silicon Nitride-Based Ceramics (Stuttgart, Germany, October 4–6, 1993). Edited by M. J. Hoffmann, P. F. Becher, and G. Petzow. Trans Tech Publications, Aedermannsdorf, Switzerland, 1994.

[17]R. L. Yeckley and K. N. Siebein, "High Temperature Cavitation of HIP Silicon Nitride"; pp. 751–65 in *Ceramic Materials and Components for Engines*. Edited by V. J. Tennery. American Ceramic Society, Westerville, OH, 1989.

[18]S. M. Wiederhorn, B. J. Hockey, D. C. Cranmer, and R. Yeckley, "Transient Creep Behavior of Hot Isostatically Pressed Silicon Nitride," *J. Mater. Sci.*, **28**, 4445–53 (1993).

[19]D. F. Carroll, S. M. Wiederhorn, and D. E. Roberts, "Technique for Tensile Creep Testing of Ceramics," *J. Am. Ceram. Soc.*, **72**, 1610–14 (1989).

[20]W. E. Luecke and J. D. French, "Sources of Strain Measurement Error in Flag-Based Extensometry," unpublished work.

[21]S. M. Wiederhorn, D. E. Roberts, T.-J. Chuang, and L. Chuck, "Damage-Enhanced Creep in a Siliconized Silicon Carbide: Phenomenology," *J. Am. Ceram. Soc.*, **71**, 602–608 (1988).

[22]"Standard Test Method for Density of Glass by the Sink-Float Comparator," Technical Report C729–75, American Society for Testing and Materials, Philadelphia, PA, 1990.

[23]C. J. Gasdaska, "Tensile Creep in an *In Situ* Reinforced Silicon Nitride," *J. Am. Ceram. Soc.*, **77**, 2408–18 (1994).

[24]C.-F. Chen, S. M. Wiederhorn, and T.-J. Chuang, "Cavitation Damage During Flexural Creep of SiAlON–YAG Ceramics," *J. Am. Ceram. Soc.*, **74**, 1658–62 (1991).

[25]T. E. Daubert and R. P. Danner, "Physical and Thermodynamic Properties of Pure Chemicals," Technical Report, Design Institute for Physical Property Data, American Institute of Chemical Engineers. Hemisphere Publishing Corp., New York, 1989.

[26]G. Porod, in *Small Angle Scattering*; Ch. 2. Edited by O. Glatter and O. Kratky. Academic Press, New York, 1982.

[27]G. Long, P. R. Jemian, J. R. Weertman, D. R. Black, H. E. Burdette, and R. Spal, "High-Resolution Small-Angle Scattering Camera for Anomalous Scattering," *J. Appl. Crystallogr.*, **24**, 30 (1991).

[28]P. R. Jemian and G. G. Long, "Silicon Photodiode Detector for Small-Angle X-Ray Scattering," *J. Appl. Crystallogr.*, **23**, 430 (1990).

[29]J. A. Potten, G. J. Daniels, and B. D. Rainford, "Particle Size Distributions from SANS Data Using the Maximum Entropy Method," *J. Appl. Crystallogr.*, **21**, 663–68 (1988).

[30]G. G. Long, S. Krueger, P. R. Jemian, D. R. Black, H. E. Burdette, J. P. Cline, and R. A. Gerhardt, "Small-Angle-Scattering Determination of the Microstructure of Porous Silica Precursor Bodies," *J. Appl. Crystallogr.*, **23**, 535 (1990).

[31]S. Krueger, G. G. Long, D. R. Black, P. R. Jemian, G. W. Nieman, and R. A. Page, "Evolution of the Pore Size Distribution in Final-Stage Sintering of Alumina Measured by Small-Angle X-ray Scattering," *J. Am. Ceram. Soc.*, **74**, 2538–46 (1991).

[32]B. N. Taylor and C. E. Kuyatt, "Guidelines for Evaluating and Expressing the Uncertainty of NIST Measurement Results," Technical Note 1297, National Institute of Standards and Technology, Gaithersburg, MD, 1994.

[33]A. A. Wereszczak, T. P. Kirkland, and M. K. Ferber, "Stress and Strain Relaxation in HIPed Silicon Nitrides," *J. Mater. Sci. Lett.*, **13**, 1469–71 (1994).

[34]P. J. Whalen, C. J. Gasdaska, and R. D. Silvers, "The Effect of Microstructure on the High-Temperature Deformation Behavior of Sintered Silicon Nitride," *Ceram. Eng. Sci. Proc.*, **11**, 633–40 (1990).

[35]R. M. Arons and J. K. Tien, "Creep and Strain Recovery in Hot-Pressed Silicon Nitride," *J. Mater. Sci.*, **15**, 2046–58 (1980).

[36]M. Gürtler and G. Grathwohl, "Tensile Creep of Sintered Silicon Nitride"; pp. 399–408 in *Creep and Fracture of Engineering Materials and Structures*. Edited by B. Wilshire and R. W. Evans. The Institute of Metals, London, U.K., 1990.

[37]F. Wakai, S. Sakaguchi, Y. Matsuno, and H. Okuda, "Tensile Creep Test of Hot-pressed Si_3N_4"; pp. 279–85 in *Ceramic Components for Engines: Proceedings of the First International Symposium 1983, Japan*. Edited by S. Sōmiya, E. Kanai, and K. I. Ando. Elsevier Science Publishing Co., London, U.K., 1986.

[38]F. F. Lange, B. I. Davis, and D. R. Clarke, "Compressive Creep of Si_3N_4/MgO Alloys, Part 3, Effects of Oxidation Induced Compositional Change," *J. Mater. Sci.*, **15**, 616–18 (1980).

[39]S. Haig, W. R. Cannon, and P. J. Whalen, "Anelastic Recovery in Crept Silicon Nitride," *Ceram. Eng. Sci. Proc.*, **13** [9–10] 1008–23 (1992).

[40]R. Krause, Jr.; personal communication.

[41]A. S. Nowick and B. S. Berry. *Anelastic Relaxation in Crystalline Solids*. Academic Press, New York, 1972.

[42]B. F. Dyson, "Constraints on Diffusional Cavity Growth Rates," *Met. Sci.*, **10**, 349–53 (1976).

[43]D. Hull and D. E. Rimmer, "The Growth of Grain-Boundary Voids Under Stress," *Philos. Mag.*, **4**, 673–87 (1959).

[44]R. Raj and P. E. D. Morgan, "Activation Energies of Densification, Creep, and Grain-Boundary Sliding in Nitrogen Ceramics," *J. Am. Ceram. Soc.*, **63**, C-143–C-145 (1981).

[45]J. R. Dryden, D. Kucerovsky, D. S. Wilkinson, and D. F. Watt, "Creep Deformation Due to a Viscous Grain Boundary Phase," *Acta Metall.*, **37** [7] 2007–15 (1989).

[46]M. M. Chadwick, D. S. Wilkinson, and J. R. Dryden, "Creep Due to a Non-Newtonian Grain Boundary Phase," *J. Am. Ceram. Soc.*, **75**, 2327–34 (1992).

[47]M. M. Chadwick, R. S. Jupp, and D. S. Wilkinson, "Creep Behavior of a Sintered Silicon Nitride," *J. Am. Ceram. Soc.*, **76**, 385–96 (1993).

[48]R. F. Cooper, D. L. Kohlstedt, and K. Chyung, "Solution-Precipitation Enhanced Creep in Solid–Liquid Aggregates Which Display a Non-zero Dihedral Angle," *Acta Metall.*, **37**, 1759–71 (1989).

[49]T. T. Gribb, S. Zhang, and R. F. Cooper, "Melt Migration and Related Attenuation in Equilibrated Partial Melts"; pp. 19–35 in *Magmatic Systems*. Academic Press, New York, 1994.

[50]F. F. Lange, "Non-elastic Deformation of Polycrystals with a Liquid Boundary Phase"; pp. 361–81 in *Deformation of Ceramic Materials*. Edited by R. C. Bradt and R. E. Tressler. Plenum Press, New York, 1975.

[51]D. R. Clarke, "High-Temperature Microstructure of a Hot-Pressed Silicon Nitride," *J. Am. Ceram. Soc.*, **72**, 1604–609 (1989).

[52]M. K. Cinibulk, H.-J. Kleebe, G. A. Schneider, and M. Rühle, "Amorphous Intergranular Films in Silicon Nitride Ceramics Quenched from High Temperature," *J. Am. Ceram. Soc.*, **76**, 2801–808 (1993).

[53]R. Raj, "Creep in Polycrystalline Aggregates by Matter Transport Through a Liquid Phase," *J. Geophys. Res.*, **87**, 4731–39 (1982).

[54]D. C. Drucker, "Engineering and Continuum Aspects of High-Strength Materials"; pp. 795–833 in *High Strength Materials*. Edited by V. F. Zackay. Wiley, New York, 1965.

[55]O. Reynolds, "On the Dilatancy of Media Composed of Rigid Particles in Contact. With Experimental Illustrations"; pp. 203–16 in *Papers on Mechanical and Physical Subjects*, Vol. 2. Cambridge University Press, Cambridge, U.K., 1901. Reprinted from December 1885 *Philosophical Magazine*.

[56]C. P. Wroth, "Soil Behaviour during Shear Existence of Critical Voids Ratios," *Engineering*, **146**, 409–12 (1958).

[57]E. B. Allison, P. Brock, and J. White, "The Rheology of Aggregates Containing a Liquid Phase with Special Reference to the Mechanical Properties of Refractories at High Temperatures," *Trans. Br. Ceram. Soc.*, **58**, 495–531 (1959).

[58]R. L. Tsai and R. Raj, "Creep Fracture in Ceramics Containing Small Amounts of a Liquid Phase," *Acta Metall.*, **30**, 1043–58 (1982).   □